Constraining the contribution of active galactic nuclei to reionization

Citation for published version:
Hassan, S, Davé, R, Mitra, S, Finlator, K, Ciardi, B & Santos, MG 2017, 'Constraining the contribution of active galactic nuclei to reionization' Monthly Notices of the Royal Astronomical Society, vol. 473, no. 1, pp. 227-240. DOI: 10.1093/mnras/stx2194

Digital Object Identifier (DOI):
10.1093/mnras/stx2194

Link:
Link to publication record in Edinburgh Research Explorer

Document Version:
Publisher's PDF, also known as Version of record

Published In:
Monthly Notices of the Royal Astronomical Society

Monthly Notices
of the
ROYAL ASTRONOMICAL SOCIETY

MNRAS **473,** 227–240 (2018) doi:10.1093/mnras/stx2194
Advance Access publication 2017 August 28

Constraining the contribution of active galactic nuclei to reionization

Sultan Hassan,[1,2]★ Romeel Davé,[1,3,4,5] Sourav Mitra,[6] Kristian Finlator,[7]
Benedetta Ciardi[2] and Mario G. Santos[1,8]

[1]*University of the Western Cape, Bellville, Cape Town 7535, South Africa*
[2]*Max-Planck-Institut für Astrophysik, Karl-Schwarzschild-Strasse 1, D-85748 Garching b. München, Germany*
[3]*South African Astronomical Observatories, Observatory, Cape Town 7925, South Africa*
[4]*African Institute for Mathematical Sciences, Muizenberg, Cape Town 7945, South Africa*
[5]*Center for Computational Astrophysics, Simons Foundation, 10010 New York, USA*
[6]*Department of Physics, Surendranath College, 24/2 M. G. Road, Kolkata 700009, India*
[7]*New Mexico State University, Las Cruces, NM 88003, USA*
[8]*SKA SA, The Park, Park Road, Pinelands 7405, South Africa*

Accepted 2017 August 23. Received 2017 July 26; in original form 2017 May 15

ABSTRACT

Recent results have suggested that active galactic nuclei (AGN) could provide enough photons to reionize the Universe. We assess the viability of this scenario using a semi-numerical framework for modelling reionization, to which we add a quasar contribution by constructing a Quasar Halo Occupancy Distribution (QHOD) based on Giallongo et al. observations. Assuming a constant QHOD, we find that an AGN-only model cannot simultaneously match observations of the optical depth τ_e, neutral fraction and ionizing emissivity. Such a model predicts τ_e too low by $\sim 2\sigma$ relative to *Planck* constraints, and reionizes the Universe at $z \lesssim 5$. Arbitrarily increasing the AGN emissivity to match these results yields a strong mismatch with the observed ionizing emissivity at $z \sim 5$. If we instead assume a redshift-independent AGN luminosity function yielding an emissivity evolution like that assumed in Madau & Haardt model, then we can match τ_e albeit with late reionization; however, such evolution is inconsistent with observations at $z \sim 4$–6 and poorly motivated physically. These results arise because AGN are more biased towards massive haloes than typical reionizing galaxies, resulting in stronger clustering and later formation times. AGN-dominated models produce larger ionizing bubbles that are reflected in $\sim\times 2$ more 21 cm power on all scales. A model with equal part galaxies and AGN contribution is still (barely) consistent with observations, but could be distinguished using next-generation 21 cm experiments such as Hydrogen Epoch of Reionization Array and SKA-low. We conclude that, even with recent claims of more faint AGN than previously thought, AGN are highly unlikely to dominate the ionizing photon budget for reionization.

Key words: galaxies: active – galaxies: high-redshift – intergalactic medium – quasars: general – quasars: supermassive black holes – dark ages, reionization, first stars.

1 INTRODUCTION

The nature of the sources driving the epoch of reionization (EoR) in the early Universe remains uncertain. It is canonically believed that star-forming galaxies have provided the bulk of the ionizing photon budget required to complete reionization (Barkana & Loeb 2001; Loeb & Barkana 2001). This is because there is a significant decrease of observed active galactic nucleus (AGN) candidates at redshifts $z > 3$, such that the contribution from star-forming galaxies is expected to well exceed that of AGN at $z > 6$ (Shapiro & Giroux 1987; Hopkins, Richards & Hernquist 2007; Glikman et al. 2011; Haardt & Madau 2012; Masters et al. 2012; Micheva, Iwata & Inoue 2017; Ricci et al. 2017; Shankar & Mathur 2017). However, there remain large uncertainties in the contribution of both star-forming galaxies and AGN to reionization. Current constraints are now consistent with a minimal contribution from very low metallicity Population III stars (e.g. Robertson, Ellis & Furlanetto 2015), but there is still the issue of the highly uncertain ionizing photon escape fraction $f_{\rm esc,*}$. Direct observations of $f_{\rm esc,*}$ are quite difficult at $z \gtrsim 4$ owing to the ubiquity of strong absorption systems that suppress Lyman continuum flux and the difficulty in removing foreground interlopers, but careful measurements generally indicate $f_{\rm esc,*}$ less than a few per cent (e.g. Grazian et al. 2016; Vasei et al. 2016), with some evidence for

---

★ E-mail: sultanier@gmail.com

Published by Oxford University Press on behalf of the Royal Astronomical Society

a higher $f_{\mathrm{esc},*}$ in lower mass galaxies (Vanzella et al. 2016; Bian et al. 2017; Grazian et al. 2017).

Theoretical models have tried to constrain $f_{\mathrm{esc},*}$ indirectly by matching models to other data, making a variety of assumptions for $f_{\mathrm{esc},*}$ such as a constant (e.g. Robertson et al. 2013; Finkelstein et al. 2015; Ma et al. 2015; Hassan et al. 2016), redshift-dependent (e.g. Kuhlen & Faucher-Giguére 2012; Mitra, Ferrara & Choudhury 2013; Finlator et al. 2015; Qin et al. 2017), mass-dependent (e.g. Gnedin 2008; Yajima, Choi & Nagamine 2011; Wise et al. 2014; Paardekooper, Khochfar & Vecchia 2015) and recently UV magnitude-dependent $f_{\mathrm{esc},*}$ (Anderson et al. 2017; Japelj et al. 2017) in order to match simultaneously various reionization constraints. The currently favoured lower value of Thomson scattering integrated optical depth ($\tau = 0.058 \pm 0.012$) measured by Planck Collaboration XLVII (2016) prefers rather sudden and late reionization scenarios, which relaxes the previously stringent constraints on the ionizing photon budget. In Hassan et al. (2017), we performed a detailed Monte Carlo Markov chain (MCMC) analysis to constrain our semi-numerical model to several EoR key observables and found that $f_{\mathrm{esc},*}$ is highly degenerate with the ionizing emissivity amplitude, leading to a best-fitting value of $f_{\mathrm{esc},\star} = 0.25^{+0.26}_{-0.13}$, which allows a substantial range but is generally higher than available (lower redshift) observations. Without a firmer understanding or direct measurement of $f_{\mathrm{esc},*}$, it is difficult to conclusively argue that star-forming galaxies can provide all the photons required for reionization.

Recently, there has been renewed interest in assessing the contribution of AGN to the reionizing photon budget. Previous estimates of the AGN contribution relied on an extrapolation to faint luminosities based on lower redshift results. But recent deep observations have enabled a more direct characterization of the faint end. Giallongo et al. (2015, hereafter G15) identified 22 faint AGN candidates at $z > 4$ and inferred a significantly steeper faint-end slope than what is seen at lower redshifts. We note that claims of such a steep faint end remain controversial; for instance Parsa, Dunlop & McLure (2017) were unable to confirm a substantial fraction of the G15 candidates based on additional multi-wavelength data. Furthermore, recent spectroscopic surveys (Kim et al. 2015; Jiang, McGreer & Ian 2016) have concluded that the observed quasar population at high redshift might not be enough to fully reionize the Universe. None the less, the differing claims have led to speculation that AGN could provide the primary ionizing photon contribution in order to keep the intergalactic medium (IGM) highly ionized (e.g. Madau & Haardt 2015). These claims further favour a late reionization scenario in which the flatness observed in the ionizing emissivity measurements by Becker & Bolton (2013) might arise naturally. In addition, they might also support the early and extended helium reionization observed by Worseck et al. (2016). Independently, Chardin, Puchwein & Haehnelt (2017) argued that the large-scale opacity fluctuations in the Lyα forest measured by Becker et al. (2015) could be explained if AGN dominate the ionizing UV background at $z \sim 6$ (see also Chardin et al. 2015). Hence, the contribution of AGN to reionization remains uncertain and potentially important or even dominant.

The idea that AGN might have driven cosmic reionization has so far been investigated mostly in terms of global quantities, such as the ability to match the optical depth or comoving ionizing emissivity constraints (e.g. Madau & Haardt 2015; Khaire et al. 2016; Mao & Kim 2016; Mitra, Choudhury & Ferrara 2016; Qin et al. 2017). It remains to be demonstrated whether AGN-driven models are able to simultaneously satisfy all the current reionization-epoch constraints. An important upcoming addition to the pantheon of constraints will be the 21 cm EoR power spectrum, which may be substantially different for AGN- versus star formation-driven reionization, if AGN and star-forming galaxies cluster in different ways as one might naively expect. An early attempt by Geil & Wyithe (2009) to assess the effect of AGN on the 21 cm power spectrum using a semi-numerical scheme concluded that the effect is likely to be small, but more recent semi-numerical models by Kulkarni et al. (2017) have suggested the opposite, that AGN produce significantly different 21 cm signal. However, the Kulkarni et al. (2017) AGN model populates AGN only in the most massive haloes using abundance matching to the halo velocity, employing the observed velocity–black hole mass relation at lower redshifts (Ferrarese 2002; Tremaine et al. 2002), which thus effectively adopts a unity duty cycle of AGN for massive haloes. However, recent results from Hyper Suprime-Cam suggest that quasars do not necessarily live in the most overdense regions where massive haloes are expected to reside, and that their duty cycle is below a few per cent (He et al. 2017). Accounting for sub-unity duty cycles inevitably drives black holes into lower mass haloes, altering the implied emissivity associated with haloes and epochs where they are not directly measured. Moreover, the G15 data suggest that the AGN driving reionization are rather faint, which may not be associated with the most massive haloes. Without a proper treatment for AGN occupancy (duty cycle) and a more comprehensive analysis of all the implications of AGN-driven reionization, it is difficult to properly assess the viability of this scenario.

In this paper, we build on our semi-numerical framework based on the SIMFAST21 code to evolve the EoR ionization field, which allows us to examine a range of EoR observations as we have done in Hassan et al. (2016, 2017). To explore the AGN contribution, we populate AGN into haloes with a more physically motivated approach that utilizes both the observed luminosity function (LF) and abundance matching, thereby generating a Quasar Halo Occupancy Distribution (QHOD); our scheme partially follows the recipe summarized in Choudhury & Ferrara (2005). We constrain our QHOD to match the G15 AGN LF fit at $z = 5.75$, and assign AGN randomly into haloes. This QHOD *predicts* a duty cycle that is close to unity for extremely massive haloes, but drops to sub-per cent values at intermediate halo masses. To obtain the AGN emissivity, we utilize the strong correlation observed between the circular velocity and black hole mass following low-redshift observations (Ferrarese 2002; Tremaine et al. 2002). We account for this additional AGN photon contribution while we evolve our SIMFAST21 density and ionization field, including the effects of recombination and time-evolving neutral fractions.

This work improves on previous efforts in several ways. First, using our SIMFAST21-based framework, we examine a wider variety of simultaneous constraints on the evolution of AGN-driven reionization, including the Thomson optical depth, the mean cosmic neutral fraction evolution and the ionizing emissivity at the end of reionization. Secondly, our model for populating quasars into haloes is more realistic than previous works because we apply constraints beyond just abundance matching, allowing us to directly constrain the duty cycle of AGN as a function of halo mass. Thirdly, we forecast upcoming 21 cm EoR power spectrum measurements from LOFAR, HERA and SKA, and illustrate how such future data might be able to constrain the fractional contribution of AGN to reionization. Our primary conclusion is that it is very difficult to reconcile purely AGN-driven reionization based on the (optimistic) G15 AGN LF measurements with current global reionization constraints. Future 21 cm data should provide a new avenue to more precisely characterize the contribution of AGN to reionization.

This paper is organized as follows: in Section 2, we describe our semi-numerical simulation and the AGN model implementation and calibration. We compare AGN with star-forming galaxies models in terms of their EoR observables, present the 21 cm predictions and discuss how future experiments can discriminate between these models in Section 3. We finally conclude in Section 4. Throughout this work, we adopt a Λ cold dark matter cosmology in which $\Omega_{\rm M} = 0.3$, $\Omega_{\Lambda} = 0.7$, $h \equiv H_0/(100\,{\rm km\,s^{-1}\,Mpc^{-1}}) = 0.7$, a primordial power spectrum index $n = 0.96$, an amplitude of the mass fluctuations scaled to $\sigma_8 = 0.8$ and $\Omega_b = 0.045$. We quote all results in comoving units, unless otherwise stated.

2 SIMULATIONS USING SIMFAST21

We use the recently developed time-integrated version of our semi-numerical code SIMFAST21 (Santos et al. 2010) that has been presented in Hassan et al. (2017). We here briefly review the simulation and defer to Santos et al. (2010) for full details about the basic algorithm, and to Hassan et al. (2016, 2017) for more information about our subsequent improvements.

The dark matter density field is generated using a Monte Carlo Gaussian approach, which is dynamically evolved into the non-linear regime via applying the Zel'Dovich (1970) approximation. The dark matter haloes are generated using the well-known excursion set formalism (ESF). In the time-integrated model, the ionized regions are identified using a similar form of the ESF that is based on comparing the time-integrated ionization rate $R_{\rm ion}$ with that of the recombination rate $R_{\rm rec}$ and the local neutral hydrogen density within each spherical volume specified by the ESF. Regions are flagged as ionized if

$$\int f_{\rm esc} R_{\rm ion}\,{\rm d}t \geq \int x_{\rm HII}\,R_{\rm rec}\,{\rm d}t + (1 - x_{\rm HII})\,N_{\rm H}, \qquad (1)$$

where $f_{\rm esc}$ is the photon escape fraction, $x_{\rm HII}$ is the ionized fraction and $N_{\rm H}$ is the total number of hydrogen atoms. This is a generalized form of the ionization condition in the time-integrated model, which can be used for any ionizing source or sink populations to run the reionization calculations. With this ionization condition, reionization occurs more suddenly compared to our previous instantaneous model developed in Hassan et al. (2016), in which the ionization condition was based on an instantaneous comparison of $R_{\rm ion}$ and $R_{\rm rec}$. The more sudden reionization is favoured by recent Planck Collaboration XLVII (2016) data, and in Hassan et al. (2017) we showed that the time-integrated ionization condition produces larger ionized bubbles, resulting in 21 power spectrum enhancement on large scales.

2.1 Sink model

Reionization, in short, is an evolving battle between ionizing photon sources and sinks. To model sinks, we must account for the clumping effects from small scales below what we can directly evolve using the large-scale SIMFAST21 code (typically, sub-Mpc scales). We thus parametrize the inhomogeneous recombination rate $R_{\rm rec}$ from high-resolution full radiative transfer hydrodynamic simulations (hereafter 6/256-RT; Finlator et al. 2015) as a function of overdensity Δ and redshift z, as follows:

$$\frac{R_{\rm rec}}{V} = A_{\rm rec}(1+z)^{D_{\rm rec}} \left[\frac{(\Delta/B_{\rm rec})^{C_{\rm rec}}}{1 + (\Delta/B_{\rm rec})^{C_{\rm rec}}}\right]^4, \qquad (2)$$

where $A_{\rm rec} = 9.85 \times 10^{-24}$ cm^{-3} s^{-1} (proper units), $B_{\rm rec} = 1.76$, $C_{\rm rec} = 0.82$, $D_{\rm rec} = 5.07$. Consistent with Sobacchi & Mesinger (2014), our recombination rate $R_{\rm rec}$ parametrization suppresses the ionization and 21 cm power spectrum on large scales. Full details about the inhomogeneous recombination $R_{\rm rec}$ parametrizations and impact on the EoR observables can be found in Hassan et al. (2016).

We note that AGN-only reionization scenarios are found to substantially heat the IGM (D'Aloisio et al. 2016; Oñorbe et al. 2017), which lowers the recombination rate. This may reduce $R_{\rm rec}$ by up to a factor of $\sim$2 in our AGN-only models, which in turn may slightly advance reionization by AGN, and hence improving the viability of AGN-only models. We do not account for this effect in our calculation since we expect it to be sub-dominant compared to other effects related to halo growth, and here simply use the same sink model to compare reionization histories produced by Galaxies versus AGN.

2.2 Source model: star-forming galaxies

For the stellar contribution, we use a parametrization obtained from combining the 6/256-RT with larger volume hydrodynamic galaxy formation simulations (Davé et al. 2013, hereafter 32/512), which have both been shown to match a range of observations including lower redshift data. From these simulations, we parametrize the non-linear ionization $R_{{\rm ion},*}$ rate as a function of halo mass $M_{\rm h}$ and redshift z as follows:

$$\frac{R_{{\rm ion},\star}}{M_{\rm h}} = A_{\rm ion}\,(1+z)^{D_{\rm ion}}\,(M_{\rm h}/B_{\rm ion})^{C_{\rm ion}}\,\exp\left(-(B_{\rm ion}/M_{\rm h})^{3.0}\right), \qquad (3)$$

where $A_{\rm ion} = 1.08 \times 10^{40}\,{\rm M}_{\odot}^{-1}$ s^{-1}, $B_{\rm ion} = 9.51 \times 10^7\,{\rm M}_{\odot}$, $C_{\rm ion} = 0.41$ and $D_{\rm ion} = 2.28$. This ionization rate is computed directly from the star formation rate (SFR) of these simulations based on stellar population models applied to star formation histories of simulated galaxies.

In Hassan et al. (2017), we considered a more generalized form of this source model, and found that constraining these parameters against several EoR observations using MCMC analysis resulted in best-fitting values that matched the above parameters to within uncertainties, thereby validating the extrapolation from the small scales of 6/256-RT and 32/512 simulations to large scales covered by SIMFAST21 simulations. We further showed that using this non-linear ionization rate relation boosts the small-scale 21 cm power spectrum as compared with models assuming a linear relation between the ionization rate and halo mass; see Hassan et al. (2016, 2017) for more details.

2.3 Source model: AGN

The new aspect of the source model for this work is the AGN ionizing photon output. We compute the ionization rate from AGN $R_{\rm ion,\,AGN}$ following partially the recipe summarized in Choudhury & Ferrara (2005). Motivated by low-redshift observations (Ferrarese 2002; Tremaine et al. 2002), the basic assumption is that the black hole mass $M_{\rm bh}$ is strongly correlated with the hosting halo's circular velocity $v_{\rm cir}$. We assume that this correlation is independent of redshift and valid during the reionization redshifts. This correlation can be written as

$$\frac{M_{\rm bh}}{{\rm M}_{\odot}} = A \left(\frac{v_{\rm cir}}{159.4\,{\rm km\,s^{-1}}}\right)^5, \qquad (4)$$

where A may be regarded as the black hole formation efficiency, which is our only free parameter in the AGN source model at fixed $f_{\rm esc,\,AGN}$. We then fix A to match the AGN ionizing emissivity constraints from G15, as we describe in Section 2.4. It is worthwhile to mention that this observed correlation (equation 4) would naturally arise if one applies a self-regulation condition on the black hole growth as previously shown by Wyithe & Loeb (2003).

For our adopted cosmology, the circular velocity $v_{\rm cir}$ of a given halo mass $M_{\rm h}$ is given by

$$\frac{v_{\rm cir}}{\rm km\,s^{-1}} = 0.014\left(M_{\rm h}\sqrt{\Omega_{\rm m}(1+z)^3+\Omega_\Lambda}\right)^{1/3}. \tag{5}$$

Having obtained the black hole mass $M_{\rm bh}$, the Eddington luminosity in the B band is given by (Choudhury & Ferrara 2005)

$$\frac{L_B}{{\rm L}_{\odot,B}} = 5.7\times10^3\,\frac{M_{\rm bh}}{\rm M_\odot}. \tag{6}$$

Given this B-band luminosity, we must now determine the ionizing photon output. Following Schirber & Bullock (2003) and Telfer et al. (2002), we assume that the spectral energy distribution for AGN takes a power-law form:

$$L_\nu = L_{912}\left(\frac{\nu}{\nu_{912}}\right)^{-1.57}, \tag{7}$$

where L_{912} is the luminosity at the Lyman limit that is given by

$$\frac{L_{912}}{\rm erg\,s^{-1}\,Hz^{-1}} = 10^{18.05}\,\frac{L_B}{{\rm L}_{\odot,B}}. \tag{8}$$

We then integrate the above over all frequencies to find the ionization rate $R_{\rm ion,\,AGN}$ as follows:

$$R_{\rm ion,AGN} = \int_{\nu_{912}}^{\infty}\frac{L_\nu}{h\nu}\,{\rm d}\nu = \frac{L_{912}}{1.57\,h}. \tag{9}$$

This explains how we compute the AGN ionization rate $R_{\rm ion,\,AGN}$ given the host halo properties.

Next, we must populate the AGN into our haloes. Here is where we make use of the G15 AGN LF. G15 evaluated this at $\lambda = 1450$ Å for several redshifts higher than $z = 4$. We then use G15 LF fit at their highest redshift $z = 5.75$ to compute the number of AGN as a function of halo mass in our simulations. G15 LF at $z = 5.75$ can be best fitted using a double power law as follows:

$$\phi = \frac{\phi^*}{10^{0.4(M_{\rm break}-M)(\beta-1.0)} + 10^{0.4(M_{\rm break}-M)(\gamma-1.0)}}, \tag{10}$$

where ϕ is the comoving AGN density, M is the absolute magnitude computed via the standard relation $M_{\rm AB} = -2.5\log_{10}(L_\nu) + 51.60$, $\log_{10}\phi* = -5.8\,{\rm Mpc^{-3}}$, $M_{\rm break} = -23.4$, $\beta = 1.66$ and $\gamma = 3.35$.

Putting this together, our procedure to populate AGN into haloes is as follows:

(i) We bin the halo catalogues as a function of halo mass, and find the average halo mass in every bin of $\Delta\log_{10}M_{\rm h} = 0.34$.

(ii) Using equations (4)–(7), we compute the corresponding AGN L_{1450} and M_{1450} of each halo mass bin.

(iii) We then obtain the number of AGN for each halo mass bin using equation (10), which turns out to always be less than the actual number of haloes; the ratio of these numbers is the duty cycle of AGN for that halo mass bin.

(iv) We randomly assign the appropriate number of AGN into haloes within that mass bin.

Note that in step (iii) one ideally may assume Poisson fluctuations around the number of AGN following McQuinn et al. (2009) QSO Method I, since the LF, in principle, yields the average number of AGN at a given magnitude bin per the simulation volume. We ignore these fluctuations for two complementary reasons. First, the number of AGN obtained from the G15 LF is very large, particularly, at the faint end ($N \sim 10^6$) around which the Poisson fluctuations can be neglected ($\sqrt{N} \sim 10^3$). Secondly, as will be seen later, our results are mainly driven by the strong AGN clustering at the faint end, and hence adding Poisson fluctuations at the very bright end (e.g. first few magnitude bins) is unlikely to affect the results since bright sources are rare. In such a situation, the average number of AGN is a very good approximation to the actual number of AGN. We then round off the resulting AGN number in order not to populate haloes with fractional AGN, but this in fact is a small correction.

Following the above procedure, we now have plausible AGN population in our simulation box at $z = 5.75$. To quantify the evolution of the AGN population, we must make a choice regarding the evolution of AGN relative to that of the haloes. Given that theoretical predictions for AGN evolution are relatively uncertain, the simplest assumption is to assume that the relationship between AGN and their host haloes does not change at $z \geq 5.75$. In other words, we assume that the QHOD is non-evolving. This is a reasonable assumption since the HOD of galaxies have been studied extensively (see Yoshikawa et al. 2001; Berlind et al. 2003, and references therein), and it is found that the HOD is nearly a redshift-independent quantity.

The QHOD as a function of halo mass $M_{\rm h}$ can directly be calculated from G15 LF fit at $z = 5.75$ (equation 10) as the ratio between the number of AGN and that of their hosting haloes for each halo mass bin. Our QHOD can be well fitted with a constant plus a power law as follows:

$$N = \left(\frac{M_{\rm h}}{2.19\times10^{12}}\right)^{0.9} + 0.023. \tag{11}$$

Note that the QHOD changes with different values of our free parameter A relating black hole mass to circular velocity, which translates into a shift in magnitudes of the AGN. Here we have used $A = 5\times10^5$, a value at which our constant QHOD AGN model is calibrated to reproduce the G15 ionizing emissivity constraints, as will be discussed next in Section 2.4.

Fig. 1 shows the QHOD computed from G15 observations at $z = 5.75$ (filled circles) and our QHOD fit in equation (11). The QHOD represents a plausible description of the AGN occupancy in their hosting haloes. Indeed, this can also be regarded as an AGN duty cycle, if one (reasonably) postulates that every halo contains a black hole but only some fraction of them are detectably active. The He et al. (2017) observations suggest a duty cycle of 0.001–0.06 for moderate-mass haloes, which is somewhat lower than our model assumes but qualitatively agrees with the trend that the duty cycle is smaller in lower mass haloes. For comparison, we also plot the QHOD at $z = 4.25$ that is computed from G15 LF at that redshift bin (open circles in Fig. 1). We notice that the QHOD data at $z = 5.75$ and 4.25 are fairly similar, differing by ∼30 per cent for all $M_{\rm h} \gtrsim 10^{10}\,{\rm M_\odot}$. This suggests that the QHOD does not evolve strongly with redshift, and motivates us to fiducially assume that the QHOD does not evolve. We will call this the ‘constant QHOD’ case. In this case, we replace equation (10) with equation (11) in step (ii) to compute directly the number of AGN in each halo mass bin at higher redshifts. Note that in step (iv) AGN assignment is completely random and redshift independent. As a result, haloes with AGN may or may not have AGN at the next time-step. This is realistic since the simulation time-step (d$z = 0.125$) is typically larger than the AGN lifetime.

As a counterpoint to this case, we also consider a model where the AGN LF is constant with time. Here, we calculate the AGN number at all redshifts based on G15 LF fit at $z = 5.75$ (equation 10). We will call this the ‘constant LF’ case. This is less realistic because the

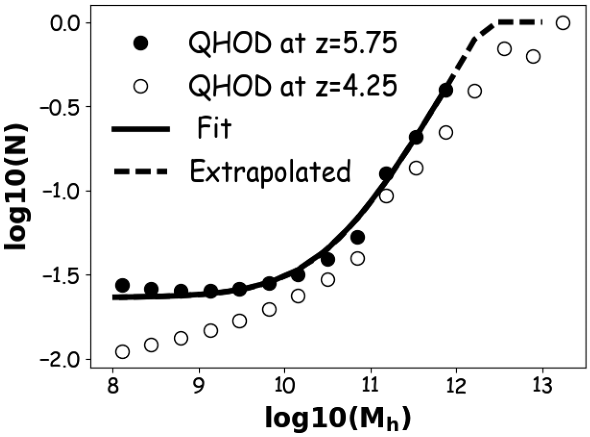

Figure 1. The QHOD as a function of halo mass $M_{\rm h}$ computed from G15 LF at $z = 5.75$ (equation 10, filled circles) and at $z = 4.25$ (open circles). The QHOD is relatively similar at these two redshift bins, providing evidence that the QHOD does not evolve strongly with redshift. The solid line represents the fitting function written in equation (11) for QHOD data at $z = 5.75$. The fitting function is extrapolated (dashed) for halo masses higher than $M_{\rm h} = 10^{12}\,{\rm M}_{\odot}$ and set to unity as an extreme occupation condition since AGN number should not exceed halo number. The QHOD increases as the $M_{\rm h}$ increases, showing that there are few AGN at massive halo mass bins. This fitting function will be used to evolve AGN from $z = 5.75$ to high redshifts in our constant QHOD AGN fiducial model.

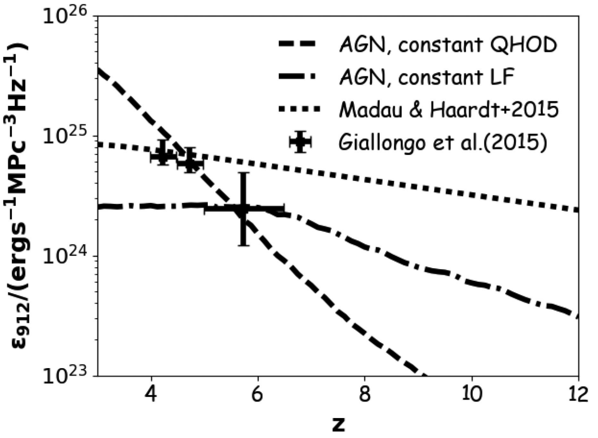

Figure 2. The comoving ionizing emissivity of AGN at 912 Å. The constant LF AGN model (dot–dashed) only matches the G15 constraints (1σ level) at $z = 5.75$, which exhibits a slowly growing emissivity evolution that is somewhat similar to the emissivity shape by Madau & Haardt (2015, dotted). The constant QHOD AGN model (dashed) yields more physical evolution as the ionizing emissivity grows rapidly, which in turn results in matching almost all of G15 data.

QHOD here increases strongly with redshift, since there are many fewer haloes at higher redshifts but the number of AGN remains fixed following the assumed constant LF. Also, observations of the AGN LF at lower redshifts ($z \lesssim 6$) exhibit significant evolution, so it seems unlikely that this evolution should suddenly cease. None the less, the emissivity evolution in this case turns out to be similar to the AGN comoving ionizing emissivity model assumed by Madau & Haardt (2015); hence, it represents an interesting contrasting case that we will examine in Section 3.

2.4 AGN source model calibration

Our next task is to calibrate the relationship between black hole mass and circular velocity via the normalization parameter A in equation (4). Observationally, this parameter is not tightly constrained and has only been measured at low redshifts.

We first calibrate the constant QHOD and constant LF AGN models to at least match the G15 ionizing emissivity constraints at $z = 5.75$ in order to verify the possibility to complete reionization solely by AGN. This we achieve by tuning the black hole formation efficiency A in our AGN models to match the total ionizing emissivity measurements at 912 Å (ϵ_{912}), which is the total escaped L_{912} of all AGN divided by the simulation comoving volume. The simulation configurations of these models are presented in Section 3 with the rest of our fiducial models. We assume $f_{\rm esc,AGN} = 100$ per cent for AGN, which is standard (e.g. Madau & Haardt 2015).

We find that the constant LF AGN model can match the G15 ionizing emissivity constraints with $A = 10^6$ whereas the constant QHOD AGN model requires $A = 5 \times 10^5$. We note that what is really constrained here is the product $Af_{\rm esc\ AGN}$, so we have the freedom to keep A fixed and tune $f_{\rm esc,\ AGN}$ instead; all our results would be unchanged. In this case, the constant QHOD and constant LF AGN models would require $f_{\rm esc,AGN} = 50$, 100 per cent at $A = 10^6$ to match the G15 constraints, respectively. Note that we do make the assumption here that the product $Af_{\rm esc,\ AGN}$ does not vary with redshift.

In Fig. 2, we show the comoving ionizing emissivity evolution obtained with the procedure discussed above. The constant LF AGN model produces a slowly growing emissivity, which is similar to the evolution expected from models in which ionizing radiation is dominated by star-forming galaxies, and similar in shape to that assumed in Madau & Haardt (2015). While matching the G15 constraints at $z = 5.75$, the constant LF AGN model underestimates the ionizing emissivity by a factor of $\sim$3 as compared with G15 constraints at $z = 4.75$ and 4.25. In contrast, the emissivity from our fiducial constant QHOD AGN model matches simultaneously G15 data at several redshift bins due to the rapidly growing emissivity evolution as expected from an AGN-dominated model. This further validates our assumption that using constant QHOD is a more physically motivated approach than using the constant LF.

Note that we have intentionally not applied a magnitude cut-off in computing the integral of emissivity (ϵ_{912}); G15 used a cut-off of $M_{1450} = -18$. At $z = 5.75$, the total comoving ionizing emissivity is $\epsilon_{912} = 2.12 \times 10^{24}\,{\rm erg\,s^{-1}\,Mpc^{-3}\,Hz^{-1}}$, whereas with a magnitude cut-off of $M_{1450} = -18$ it becomes $\epsilon_{912} = 1.58 \times 10^{24}\,{\rm erg\,s^{-1}\,Mpc^{-3}\,Hz^{-1}}$. This shows that those fainter AGN contribute $\sim$25 per cent to the total emissivity, which is modest but not negligible. We include this in order to check whether including all faint AGN would allow reionization completion to be consistent with neutral fraction and optical depth constraints. This means that we are effectively studying an optimal case for reionization by AGN, since those fainter than $M_{1450} > -18$ might already be a part of the galaxy population as discussed in Chardin et al. (2017), due to the overlap between the galaxy and AGN LF at this faint limit. Applying a magnitude cut-off would suppress the ionizing emissivity and further delay reionization.

In summary, we have described our procedure to obtain the ionizing emissivity of AGN as a function of halo mass, and then populate AGN into haloes within SIMFAST21 via constraining the halo occupancy of AGN (QHOD) using the G15 AGN LF. The total emissivity is calibrated to match that observed by G15 at $z = 5.75$, which fixes our free parameter relating black hole mass to halo circular velocity. Our fiducial model assumes a constant QHOD, and we will also

Table 1. Summary of models considered in Section 3 to compare between the AGN and star-forming galaxies impacts on different reionization constraints. Columns (from left to right) are: models' names, the photon escape fractions from star-forming galaxies $f_{\rm esc,*}$ and AGN $f_{\rm esc\ AGN}$, the ionization rate used in equation (1), the optical depth τ_e and reionization redshift $z_{\rm reion}$ defined at neutral fraction limit $x_{\rm HI} < 10^{-3}$.

Model	$f_{\rm esc,*}$	$f_{\rm esc\ AGN}$	Ionization rate	τ_e	$z_{\rm reion}$
Galaxies	0.25	0.0	$f_{\rm esc,*}\, R_{\rm ion,*}$	0.057	7.5
constant QHOD AGN	0.0	1.0	$f_{\rm esc,AGN}\, R_{\rm ion,AGN}$	0.036	5.0
50–50	0.125	0.5	$f_{\rm esc,*}\, R_{\rm ion,*} + f_{\rm esc,AGN}\, R_{\rm ion,AGN}$	0.049	6.5
constant LF AGN	0.0	1.0	$f_{\rm esc,AGN}\, R_{\rm ion,AGN}$	0.048	4.0

consider a constant AGN LF. We now study the predictions of our model for reionization observables, and compare the results with our previous SIMFAST21 models where we considered only star-forming galaxies.

3 EOR OBSERVABLES

3.1 SIMFAST21 runs

We run all of our EoR realizations using the time-integrated model (Hassan et al. 2017) to establish a proper comparison between the different source models. Using the same density field and halo catalogues generated in a box size $L = 300$ Mpc and $N = 560^3$ number of cells, we run four different EoR models based on different ionization sources as follows (and summarized in Table 1).

(i) *Galaxies*: This model only considers ionizing photons emitted by star-forming galaxies using equation (3) with parameters: $f_{\rm esc,*} = 0.25$, $A_{\rm ion} = 4.27\times 10^{39}$, $C_{\rm ion} = 0.44$. These parameters are suggested by our recent MCMC analysis in Hassan et al. (2017) to match simultaneously various EoR constraints including the SFR densities at several redshift bins as compiled by Bouwens et al. (2015a), integrated ionizing emissivity at $z \sim 5$ by Becker & Bolton (2013) and Planck Collaboration XLVII (2016) optical depth.

(ii) *Constant QHOD*: This is our fiducial AGN model in which the AGN are the only source for ionizing radiation using $f_{\rm esc,\,AGN} = 1.0$, and our QHOD fitting function (equation 11) is computed from G15 LF fit at $z = 5.75$.

(iii) *50–50*: This model contains an equal contribution from the *Galaxies* and *constant QHOD* models; specifically we use $f_{\rm esc,*} = 0.125$ and $f_{\rm esc,\,AGN} = 0.5$.

(iv) *Constant LF*: This is our alternative AGN model that uses the actual LF fit of G15 at $z = 5.75$ to compute the number of AGN at all redshifts, with $f_{\rm esc,\,AGN} = 1.0$.

3.2 Ionizing emissivity

We begin by comparing the integrated ionizing emissivity $\dot{N}_{\rm ion}$ of these models, which is the total number of ionizing photons per second per comoving volume. We compare our models with results from Qin et al. (2017) based on the DRAGONS simulation, which uses the MERAXES semi-analytic galaxy formation model built upon the TIAMAT N-body simulation. The Qin et al. (2017) model is able to track the growth of central supermassive black holes and reproduce a wide range of observations including the observed quasar LF from $z \sim 0.6$ to 6. Their model predicts that AGN contribution to EoR is minimal, so it is interesting to compare our AGN emissivity with theirs.

Fig. 3 shows the redshift evolution of the comoving integrated ionizing emissivity $\dot{N}_{\rm ion}$, in units of 10^{51} s^{-1} Mpc^{-3}, for our four models. For the Qin et al. (2017) models (blue lines), we show their full Galaxies+AGN model as well as their AGN-only contribution. At $z \lesssim 5$, we show the observational constraints from Becker & Bolton (2013) inferred from Lyα forest measurements.

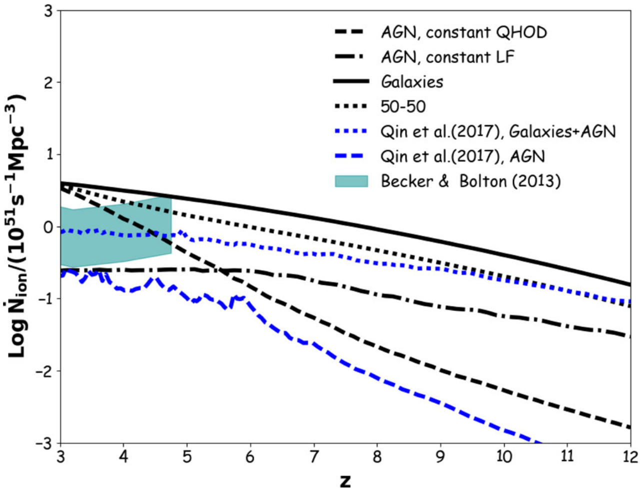

Figure 3. The comoving integrated ionizing emissivity as a function of redshift. The Becker & Bolton (2013) measurements are shown with the cyan shaded area (1σ level). The emissivity evolution in our Galaxies model (black solid) and that in Galaxies+AGN model (dotted blue) by Qin et al. (2017) are similar with an amplitude difference due to these models' basic framework and assumption (see the text for details). The emissivity in constant LF AGN model (dot–dashed black) grows slowly similar to galaxy-driven EoR models, which reflects the poor assumption of using a fixed AGN LF through all times. Our fiducial constant QHOD AGN model (dashed black) produces reasonable emissivity evolution with a steep decline towards high redshift, consistent with the AGN model (dashed blue) by Qin et al. (2017).

Our Galaxies model skirts the upper limit of Becker & Bolton (2013) constraints while simultaneously calibrated to reproduce the Bouwens et al. (2015a) SFR and Planck Collaboration XLVII (2016) optical depth, as discussed in Hassan et al. (2017). Adopting a mildly redshift-dependent or even mass-dependent $f_{\rm esc,*}$ would permit a better match with the amplitude and flat redshift dependence of the Becker & Bolton (2013) emissivity measurements, as suggested by Mutch et al. (2016), without much altering the Thomson optical depth.

Our fiducial constant QHOD model shows a much more rapid growth of ionizing emissivity with time than the Galaxies model, which matches the Becker & Bolton (2013) ionizing emissivity at the upper end of the observed redshift range but overshoots the low end. In this model, the AGN contribution overtakes the Galaxies contribution at $z \sim 3$, which is in agreement with what is typically inferred (e.g. Haardt & Madau 2012).

We further see that our 50–50 model (dotted black in Fig. 3) is similar and much closer to the Galaxies model than to the constant QHOD model. This indicates that the contribution from star-forming galaxies dominates the ionizing emissivity while AGN contribution is minor.

Finally, the constant LF model shows a relatively shallow evolution, approximately parallel to the Galaxies case but significantly lower in amplitude. This falls just below the ionizing emissivity data at $z \lesssim 5$.

The blue dotted and dashed lines show the evolution of the emissivities from the Qin et al. (2017) model, with the latter showing only the contribution from AGN. Their AGN contribution shows a similar redshift dependence on our constant QHOD model, which further supports the validity of this assumption, at least down to $z \sim 6$. It is possible that our assumption breaks down at $z \lesssim 5$ as their AGN contribution flattens, and if ours did this, then the agreement with the observed evolution of the emissivity would improve. However, DRAGONS also predicts that galaxies dominate the ionizing photon budget at all redshifts, which may be contrary to studies of the hardness of the ionizing background in the $z \sim 2$–4 IGM (e.g. Schaye, Carswell & Kim 2007; Oppenheimer, Davé & Finlator 2009).

The emissivity evolution in our Galaxies model is similar to that from the Galaxies+AGN model by Qin et al. (2017), whereas there is a difference in the amplitude due to these models' differences in the $f_{\rm esc}$ treatment (constant versus redshift dependent). As previously noted, the constant LF AGN model shows a slowly growing emissivity similar to those of our Galaxies model and Galaxies + AGN model by Qin et al. (2017).

In summary, our fiducial constant QHOD AGN model matches the Becker & Bolton (2013) emissivity measurements reasonably well, at least at $z \sim 5$, but shows a dramatically different redshift evolution compared to our Galaxies and constant LF models. The Qin et al. (2017) DRAGONS model shows an evolution during reionization that is consistent with our constant QHOD model for their AGN component, and with our Galaxies model for their overall emissivity (which is dominated by galaxies), but somewhat lower in amplitude in each case. All these models are broadly in agreement with the emissivity measures at $z \sim 5$ given current uncertainties.

3.3 Global ionization history and optical depth

We now explore our model predictions for other current observational constraints on the global evolution of reionization, particularly the evolution of the volume-weighted neutral fraction $x_{\rm HI}$ and the integrated Thomson optical depth to electron scattering to the cosmic microwave background (CMB) τ_e.

Fig. 4 shows a comparison between our models in terms of their global ionization history, as characterized by the volume-weighted average neutral fraction $x_{\rm HI}$. We see that our Galaxies and 50–50 models are consistent with several Lyα forest measurements (shaded areas from Fan, Carilli & Keating 2006; Becker et al. 2015; Bouwens et al. 2015b and orange upper limits by McGreer, Mesinger & DOdorico 2015). While both are consistent with data, the 50–50 model delays reionization by $\Delta z \sim 1.0$, owing to the fact that galaxies are the main driver of reionization as discussed in the previous section and their contribution has been halved in this model.

Turning to our AGN-driven reionization models, we see that both the constant LF and constant QHOD reionize the Universe very late, with $x_{\rm HI} < 10^{-3}$ not occurring until $z \sim 4$ and $z \sim 5$, respectively. This is highly inconsistent with the Bouwens et al. (2015b) constraints as seen in Fig. 4, as well as direct observations of the Lyα forest in quasars at these epochs (Fan et al. 2006; Becker et al. 2015). The constant LF AGN model starts reionization earlier than constant QHOD AGN model due to its higher emissivity at high redshifts (Fig. 3). This too-late reionization strongly suggests that AGN are unable to drive the bulk of reionization, when constrained to match the observed ionizing emissivity after the end of reionization ($z \sim 5$).

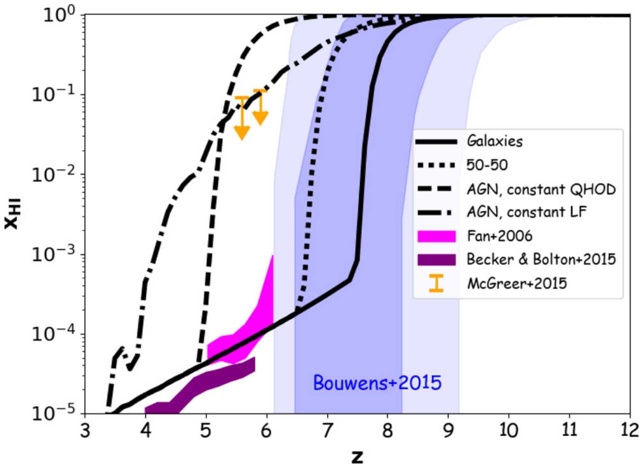

Figure 4. The volume-weighted averaged neutral fraction evolution as a function of redshift. The shaded areas: magenta, purple and light blue are from Lyα forest measurements by Fan et al. (2006), Becker et al. (2015), and several AGN and Lyα constraints (1σ and 2σ) as compiled by Bouwens et al. (2015b), respectively. We also compare to the model-independent upper limits by McGreer et al. (2015, orange error bars) using Lyα and Lyβ forest. It is evident that Galaxies (solid) and 50–50 (dotted) models are consistent with all observations, which implies the importance of including star-forming galaxies to match with observations. Our AGN models, constant LF (dot–dashed) and constant QHOD (dashed), both complete reionization very late. This indicates that AGN contribution to cosmic reionization is minor.

As mentioned earlier, all models use the time-integrated ionization condition (equation 1) to identify the ionized regions in the ESF. We showed in Hassan et al. (2017) that this ionization condition results in a more sudden reionization as opposed to our previous instantaneous model (Hassan et al. 2016) that yields an extended reionization scenario. From Fig. 4, all models yield a fairly sudden reionization, consistent with our previous results, except the constant LF AGN model that shows an extended reionization. This is because the fixed LF likely overestimates the number of AGN at high redshifts, and furthermore the source population does not grow in concert with the growing sink population, which delays reionization.

Fig. 5 shows the evolution of the Thomson scattering optical depth (τ_e) as a function of redshift in these models. The Galaxies model is consistent with the recent Planck Collaboration XLVII (2016) measurements (red shaded areas), mostly because it was constrained to do so via MCMC. The 50–50 and constant LF yield a lower optical depth of about $\tau \sim 0.049$, consistent with the lower limit of 1σ level. However, the optical depth obtained by our fiducial constant QHOD AGN model is very low ($\tau \sim 0.036$) at the lower limit of the 2σ level. Essentially, this model does not produce enough early photons in order to obtain a sufficient ionized path-length to the CMB.

One might question why Madau & Haardt (2015) were able to match these constraints based on the G15 model and thereby argue for purely quasar-driven reionization, whereas we reach an opposite

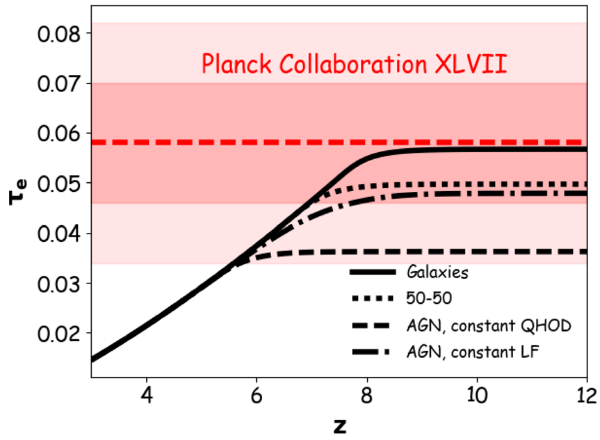

Figure 5. Thomson scattering optical depth evolution as a function of redshift. The shaded red dark and light areas represent the 1σ and 2σ levels of the recent Planck Collaboration XLVII (2016) optical depth measurement whereas the dashed red horizontal line marks the measured *Planck* value ($\tau = 0.058 \pm 0.012$). The Galaxies model (solid) is consistent with the actual optical depth value. The 50–50 and constant LF models obtain a lower optical depth of $\tau \sim 0.049$, matching the lower 1σ level of *Planck*. Our fiducial constant QHOD AGN models produce a very low optical ($\tau \sim 0.036$) that lies at the lower limit of 2σ level.

conclusion. There are two main differences. First, Madau & Haardt (2015) made a rough fit to the ionizing emissivity, which resulted in a much flatter redshift dependence than we obtain from our constant QHOD model, more like our constant LF model except higher in amplitude by ∼×2–3 (see Fig. 2). Indeed, our constant LF model results in an ionizing emissivity evolution much like theirs, and is consistent (albeit marginally) with τ_e. Secondly, Madau & Haardt (2015) purely relied on counting emitted photons, and did not account for an evolving spatially clustered nature of sinks, which absorb more photons, and hence retard reionization particularly at early epochs compared to a spatially homogeneous clumping factor model. These differences result in substantially more neutral gas at early epochs in our model, and lead to strong disagreement with the measured τ_e as well as $x_{\rm HI}$.

Our 50–50 model can plausibly match the constraints within current 1σ uncertainties. Recall that for our Galaxies model, Hassan et al. (2017) found $f_{\rm esc} = 0.25^{+0.26}_{-0.13}$, which means that the galaxy contribution alone in the 50–50 model corresponds to an escape fraction that is at the 1σ bound allowed by the MCMC fit. Correspondingly, the predicted τ_e and the redshift of reionization are near the 1σ low end of their respective allowed observational ranges.

The Qin et al. (2017) AGN model yields an optical depth of $\tau \sim 0.025$, corresponding to an end of reionization at $z \sim 3$. Our constant QHOD AGN model would obtain similar results if a magnitude cut-off had been implemented in the ionizing emissivity integral to exclude the very faint AGN. Even with our more favourable case of reionization by AGN, reionization still occurs very late.

Overall, we find that our constant QHOD model that is constrained to match the AGN emissivity of G15 can adequately match the global ionizing emissivity at $z \sim 5$, but strongly fails to reionize the Universe by $z \sim 6$ and produces too low Thomson optical depth. A constant LF model does somewhat better at matching constraints, but the underlying assumption is not physically well motivated, does not match the observed emissivity evolution from $z \sim 6 \rightarrow 4$ and is inconsistent with the self-consistent calculations of Qin et al. (2017). A 50–50 model is still within the allowed bounds of the observations considered here, but any larger contribution from AGN would be disfavoured – and we reiterate that our AGN model is already pushed towards increasing the AGN emissivity as much as possible. Our $x_{\rm HI}$ and τ_e constraints for all these models are listed in Table 1. Our results thus suggest that AGN-dominated reionization is highly unlikely, and therefore that galaxies dominate the ionizing photon budget during the EoR.

3.4 EoR topology

We have shown that our AGN-only models are highly disfavoured given current observational data. However, a 50–50 model is still permissible, if only marginally. Clearly, increasing the precision of current measures should in principle enable more stringent constraints on the relative contribution of AGN and star-forming galaxies to reionization. But we can also appeal to other aspects such as the topology of reionization in order to discriminate between models. This will be particularly fruitful in the era of 21 cm EoR experiments, which will quantify the power spectrum of neutral hydrogen on large scales. In this section, we discuss the topology of neutral gas in our various models, and in the following section we will quantify this by forecasting the 21 cm power spectrum for upcoming experiments.

We first investigate these models' differences in terms of their ionization field maps. We choose to compare these models' maps at a fixed neutral fraction, since we have shown in Hassan et al. (2017) that the 21 cm fluctuations are more sensitive to the topology of the ionization field while the density field contribution is secondary. This then allows us to compare the topology even though the actual redshift where a given ionization occurs varies substantially between models.

Fig. 6 shows 2D maps of the ionization field of all models at different neutral fractions ($x_{\rm HI} \approx 0.25, 0.5, 0.75$), projected through the entire volume. Note that the redshifts at which this occurs are much later for the AGN-only models, consistent with their late reionization. Our Galaxies model shows a range of bubble sizes, with many small bubbles around low-mass galaxies that have low clustering. The largest bubbles towards the end of reionization span ∼100 Mpc, in agreement with many previous studies (e.g. Barkana & Loeb 2004; Furlanetto, Zaldarriaga & Hernquist 2004; Mesinger, Furlanetto & Cen 2011; Zahn et al. 2011; Iliev et al. 2014; Majumdar et al. 2014). It is clear that there will be significant power on all scales owing to this topology.

The constant QHOD and constant LF AGN models show fairly similar H II bubble sizes and distributions. Compared to the Galaxies case, there are fewer small bubbles owing to the fact that AGN tend to populate more massive haloes than the typical galaxy contributing to reionization in the Galaxies model. However, there are still some small haloes hosting small bubbles even in the AGN case. This contrasts with the Kulkarni et al. (2017) AGN model where AGN are assigned only in the massive haloes using a circular velocity cut-off, and thus their model does not yield any small-scale H II regions (see their fig. 2). None the less, because the duty cycle of AGN in our model is very low in low-mass haloes, many fewer small bubbles are seen compared to the Galaxies case.

For large ionizations, the ionization maps of the constant QHOD and constant LF AGN models display larger H II regions as compared with those of Galaxies model. This is necessary to compensate for the lack of numerous small bubbles, in order to achieve a similar neutral fraction. This is driven by the strong AGN clustering as suggested by the input G15 LF at its faint end.

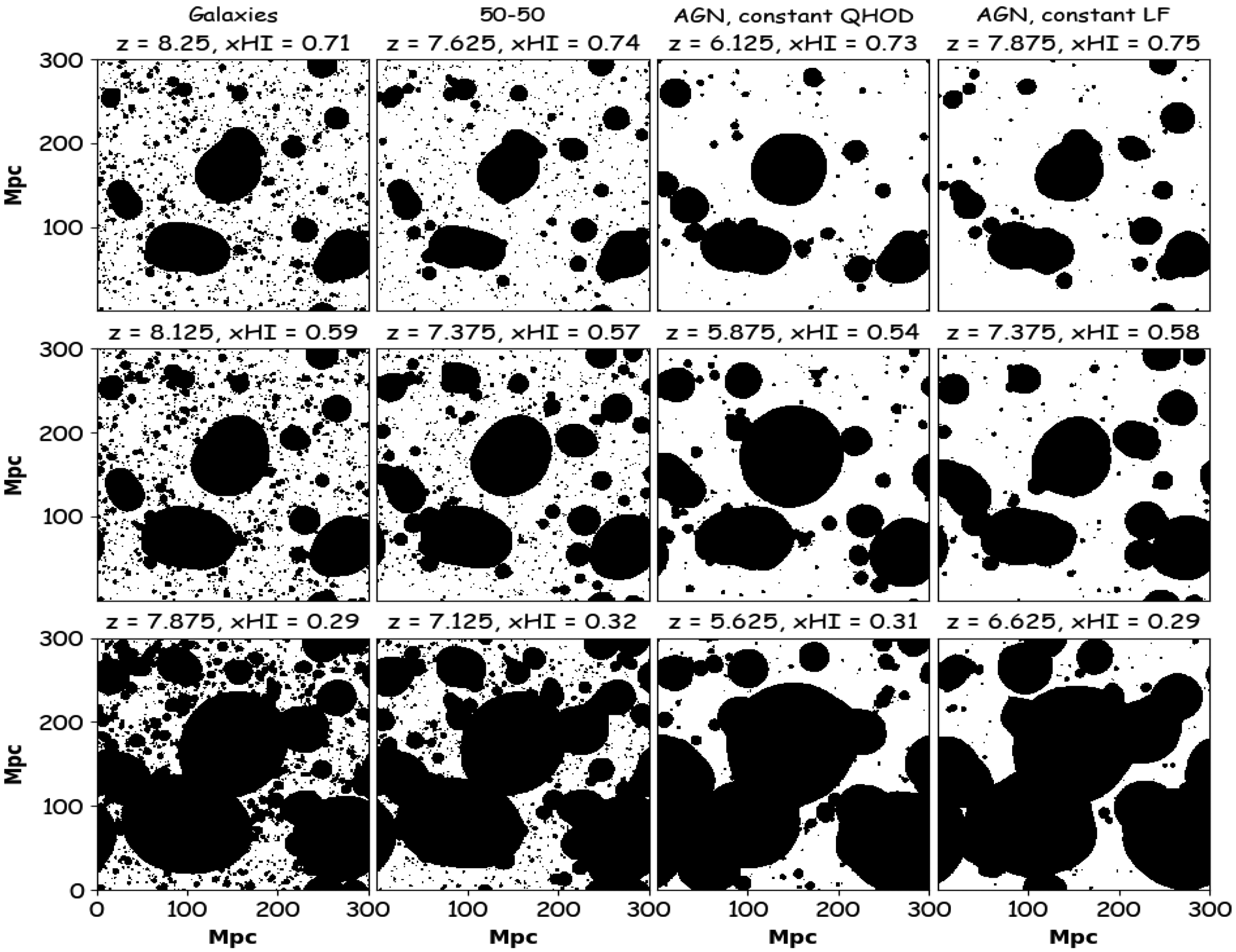

Figure 6. Slices of the ionization box each of a size 300 × 300 × 0.535 Mpc^3 from our four models at different stages of reionization. Top to bottom: $x_{\mathrm{HI}} \approx$ 0.25, 0.5, 0.75. Left to right: Galaxies, 50–50, constant QHOD, constant LF models. White and black represent neutral and ionized regions, respectively. The constant QHOD and constant LF AGN models show large H II bubbles as compared to Galaxies model. The Galaxies and 50–50 models show similar topology, indicating that galaxies play a stronger role in determining the H II regions' properties. Actual redshifts and neutral fractions are quoted on top of each map.

The 50–50 model is, not surprisingly, intermediate between the Galaxies and AGN-only models. The small bubbles are less prominent owing to the lower $f_{\mathrm{esc},*}$. The maximum bubble sizes are comparable to but slightly larger than in the Galaxies model. Hence, the star-forming galaxies tend to drive the topology even when substantial AGN are present. This comes from the facts that each halo mass bin (magnitude bin) includes fewer AGN than the number of possible hosting haloes as implied by the AGN duty cycle estimates (e.g. Shankar, Weinberg & Miralda-Escudé 2009), and hence star-forming galaxies would overcome the impact of those fewer AGN on the ionization field topology. The difference between AGN (constant QHOD and constant LF) and star-forming galaxies (Galaxies and perhaps 50–50) dominated models increases as reionization proceeds and becomes clear at late stage of reionization (bottom row for $x_{\mathrm{HI}} \sim 25$ per cent of Fig. 6). We expect these trends to be reflected quantitatively in their 21 cm power spectra.

3.5 The 21 cm power spectrum

Using the ionization fields of these models at fixed neutral fractions (Fig. 6), we now compute our key EoR observable, namely the 21 cm power spectrum. Assuming that the spin temperature is much higher than the CMB temperature, the 21 cm brightness temperature takes the following form:

$$\delta T_{\mathrm{b}}(\nu) = 23 x_{\mathrm{HI}} \Delta \left(\frac{\Omega_{\mathrm{b}} h^2}{0.02}\right) \sqrt{\frac{1+z}{10}\,\frac{0.15}{\Omega_{\mathrm{m}} h^2}} \left(\frac{H}{H + \mathrm{d}v/\mathrm{d}r}\right) \mathrm{mK}, \quad (12)$$

where $\mathrm{d}v/\mathrm{d}r$ is the comoving gradient of the line-of-sight component of the peculiar velocity. Using this equation, it is straightforward to create the 21 cm brightness temperature boxes from which we compute the 21 cm power spectrum as follows: $\Delta^2_{21} \equiv k^3/(2\pi^2\, V)\langle|\delta T_{\mathrm{b}}(k)|^2_k\rangle$.

In top panels of Fig. 7, we show a comparison between our models' predicted 21 cm power spectrum and those predicted with the AGN-dominated models of Kulkarni et al. (2017). Bottom panels show the ratio of each model 21 cm power spectrum to the Galaxies model, in order to clearly display the models' differences as a function of the scale k. Consistent with the ionization maps (Fig. 6), the Galaxies model has less power than the AGN-only models, which at a fixed x_{HI} are themselves rather similar. This shows that the 21 cm power spectrum is somewhat insensitive to the method by which we populate AGN (constant QHOD versus constant LF), even though

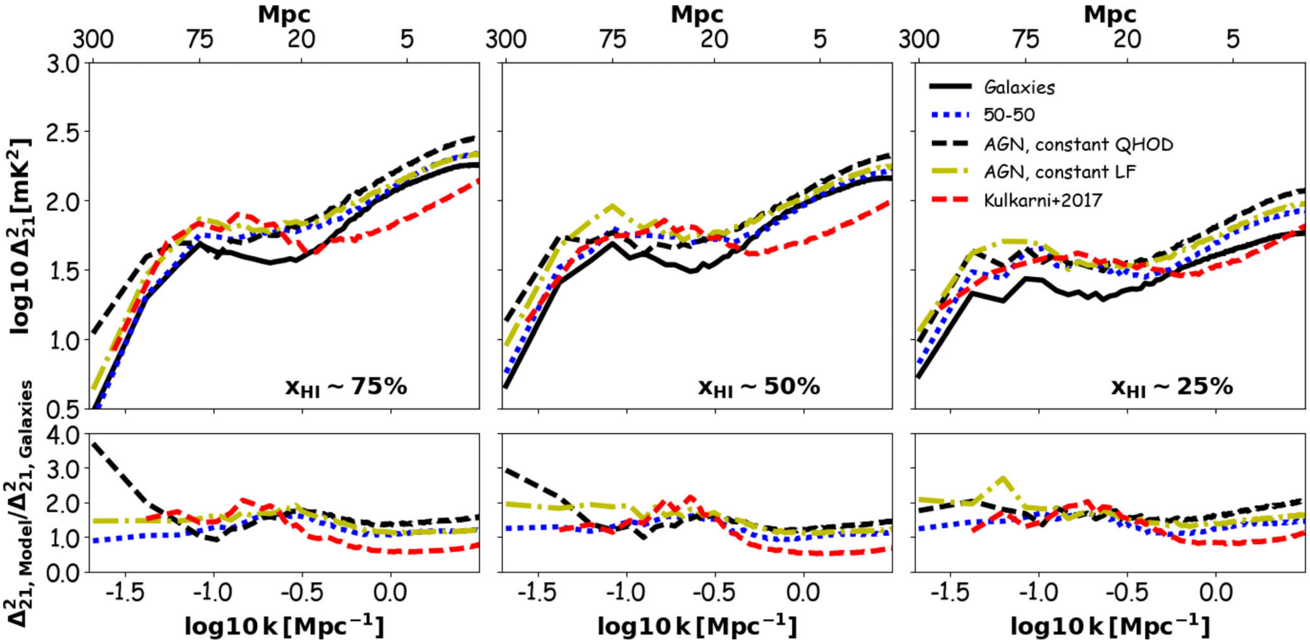

Figure 7. Top: the 21 cm power spectrum comparison between all models at fixed neutral fractions. We also compare to the recent AGN model developed by Kulkarni et al. (2017, dashed red). The Galaxies (black solid) and 50–50 (dotted blue) models produce similar power spectra on small and large scales, particularly at intermediate ($x_{\rm HI} \sim 0.5$) and early ($x_{\rm HI} \sim 0.75$) stages of reionization. Likewise, the constant QHOD (dashed black) and constant LF (dot–dashed yellow) AGN models yield similar power spectra. The AGN models produce power spectra that are higher by a factor of ∼×1.5–2 than the Galaxies model. The power spectra obtained by Kulkarni et al. (2017) AGN model agree with our AGN models relatively on large scales but they are lower by a factor of ∼×2–2.5 on small scales, due to these models' differences in populating AGN into haloes (see the text for details). Bottom: the ratio of each model power spectrum to that of Galaxies as a function of the scale k, which shows the difference between each model and Galaxies.

there is a clear difference in the reionization histories due to differences in the ionizing emissivity evolutions (see Figs 3 and 4). Relative to the Galaxies case, at early epochs the differences with the AGN-only models peak at intermediate scales ($k \sim 0.3$–0.1), typical of the AGN bubble sizes. At later epochs, however, there is not much scale dependence on the variation, and the AGN models are simply about a factor of 1.5–2 higher than the Galaxies model, owing to the stronger clustering of G15 AGN observations.

The 50–50 models yield similar 21 cm power spectra both on small and large scales to the Galaxies case at the early ($x_{\rm HI} \sim 0.75$) and intermediate ($x_{\rm HI} \sim 0.5$) stages of reionization. This confirms our previous finding that star-forming galaxies are dominant in determining the ionized regions' properties and hence their associated 21 cm fluctuations during the early stages of reionization. At later stages, there is an increasing difference between the 50–50 model and the Galaxies case, owing to the increased contribution of AGN at later epochs. Hence, it may be optimal to look at the later stages of reionization in order to obtain more quantitative constraints on the fractional contribution of AGN.

Our AGN models agree with the Kulkarni et al. (2017) AGN model reasonably well for the large-scale 21 cm power spectrum, while their small-scale power is suppressed by a factor of ∼× 2–2.5 relative to ours. As mentioned before in Section 3.4, our AGN model yields small-scale ionized regions owing to populating AGN randomly at all halo mass bins (magnitude bins) into their hosting haloes using the actual number of AGN as suggested by the G15 LF observations, as opposed to a unity duty cycle in massive haloes in the Kulkarni et al. (2017) AGN model. By constraining our LF to that observed, our AGN model predicts a non-unity duty cycle, which occasionally populates small haloes with AGN and thus boosts the 21 cm power spectrum on small scales.

3.6 Forecasting 21 cm power spectra to constrain AGN models

Our work has shown that AGN-driven EoR models are photon-starved, in agreement with many others, and as such plausible AGN models are unlikely to fully drive reionization. None the less, a substantial AGN contribution such as in our 50–50 model is still allowable given current data, which begs the question, will future 21 cm data provide more stringent constraints on the contribution of AGN to reionization?

To answer this question, we focus our analysis on three different low-frequency radio interferometer designed to measure the 21 cm EoR power spectrum: the Low Frequency Array (LOFAR),[1] the Hydrogen Epoch of Reionization Array (HERA)[2] and the Square Kilometre Array (SKA-low).[3]

To forecast the power spectra for these facilities, we use the same recipe presented in Hassan et al. (2017), outlined as follows: we first select the redshift (observed frequency) at which we compute the 21 cm power spectrum for each model. To establish a proper comparison, we operate these three array designs, with parameters summarized in Table 2, in a drift-scanning mode for 6 observing hours per day for 180 d at 8 MHz bandwidth. We then add the total uncertainty that includes the thermal noise and sample variance using the 21cmSense,[4] a package for calculating the sensitivity of 21 cm experiments to the EoR power spectrum. We refer to Parsons et al. (2012) for basics of the radio interferometer sensitivities, to Pober et al. (2013, 2014) for more details on observation strategies

---

[1] http://www.lofar.org/

[2] http://reionization.org

[3] https://www.skatelescope.org

[4] https://github.com/jpober/21cmSense

Table 2. Summary of parameters used in 21 CMSENSE package to obtain the thermal noise sensitivity for each experiment. Columns (from left to right) are: experiments' names, designs, antenna diameter, total collecting area and the receiver temperature. The sky temperature is given by $T_{\rm sky} = 60\lambda^{2.55}$ K.

Experiment	Design	Diameter (m)	Collecting area (m^2)	Receiver temperature (mK)
LOFAR	48 tiles of bow-tie high-band antennas	30.75	35 762	140 000
HERA	331 hexagonally packed antennas	14	50 953	100 000
SKA	866 compact core antennas	35	833 189	100 $T_{\rm sky}$ + 40 000

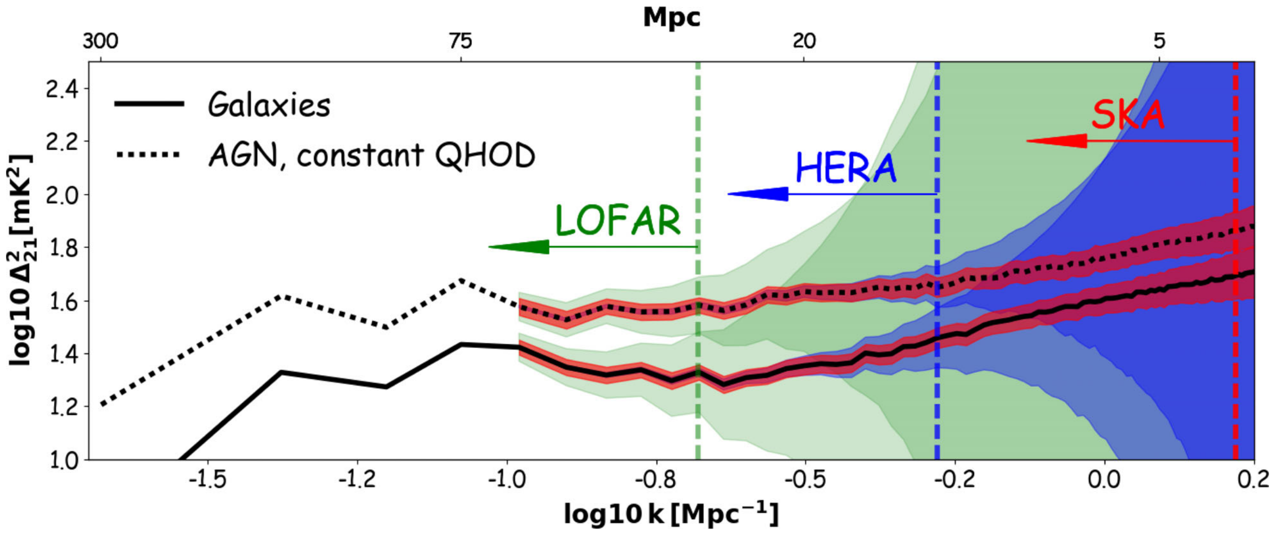

Figure 8. Mock 21 cm EoR power spectrum observations using the same telescope designs and configurations at $z = 8$ and $x_{\rm HI} \sim 30$ per cent from our Galaxies (black solid) and constant QHOD AGN (black dashed, tuned to match Galaxies model optical depth τ) models. Shaded areas show the 1σ error bars obtained using 21 CMSENSE package for our constructed EoR arrays: SKA (red), HERA (blue), LOFAR (green). Vertical dashed lines represent the scale at which a specific experiment may distinguish between these models (the scale at which error bars overlap from a specific experiment). Future 21 cm observations by these experiments will be able to discriminate between these models at their corresponding sensitivity limits.

and foreground removal models, and to Hassan et al. (2017) for the experiments designs and configurations. We only change the foreground removal method to use the optimistic model developed in Pober et al. (2014) in which the foreground wedge extends to the full width at half-maximum of the experiments' primary beam. This will extend our analysis to cover more large scales than using a moderate model in which foreground wedge extends only to 0.1 $h\,\mathrm{Mpc}^{-1}$ beyond horizon limit.

From Fig. 7, we notice that the large variations between the Galaxies and constant QHOD AGN models occur at the late stages of reionization ($x_{\rm HI} \sim 25$ per cent) when the H II bubbles begin to overlap. We thus create our 21 cm mock observations at these epochs. Since the reionization occurs very late in the constant QHOD AGN model (see Fig. 4), we re-tune the model (using $A = 1.25 \times 10^7$, which we note would substantially overproduce the ionizing emissivity constraints) to match the optical depth as obtained by Galaxies model. We then perform our 21 cm mock observations at $z = 8$ and $x_{\rm HI} \sim 0.3$ for both models in order to conduct a comparison at the same redshift and neutral fraction.

Fig. 8 shows a 21 cm mock observation comparison at $z = 8$ ($x_{\rm HI} \sim 0.3$) between Galaxies and the re-tuned constant QHOD AGN models. The shaded area shows the total uncertainties (1σ level) expected from the experimental designs summarized in Table 2 using the 21CMSENSE package. The vertical lines mark the scale at which the 1σ error bars from a specific experiment overlap, corresponding to the sensitivity limit for each experiment where the models can be distinguished.

Given that it can only probe relatively large scales, LOFAR will have some difficulty discriminating between the Galaxies and constant QHOD models, as they lie within $\sim 2\sigma$ of each other. However, HERA should be able to distinguish between these models rather well on scales above about 10 Mpc, and the larger baselines of SKA-low will enable discrimination to significantly smaller scales. From Fig. 8, we see that LOFAR, HERA and SKA can discriminate between these models during the later stages of reionization at scales of $k < 0.21\,\mathrm{Mpc}^{-1}$ (>30 Mpc), $k < 0.53\,\mathrm{Mpc}^{-1}$ (>12 Mpc) and $k < 1.66\,\mathrm{Mpc}^{-1}$ (>4 Mpc), respectively.

The fact that HERA and SKA can easily discriminate AGN-only and Galaxies-only models suggests that it may be possible to constrain the fractional contribution of AGN using such data. We thus repeat the same steps above, except now for the 50–50 model, tuned to match Galaxies τ_e.

Fig. 9 shows a forecasting comparison between the Galaxies and 50–50 models. Since the 50–50 model yields 21cm power amplitude that is closer to Galaxies than constant QHOD model does, the scales at which experiments overlap are shifted towards large scales (compare vertical dashed lines in Fig. 8 versus Fig. 9). This shows that LOFAR is unlikely to discriminate between these models, unless a very optimistic foreground removal is applied to detect the signal on large scales [$k < 0.12\,\mathrm{Mpc}^{-1}$ (>53 Mpc)], which are highly contaminated by foregrounds (Pober et al. 2014). Given a successful foreground removal, HERA and SKA can discriminate between the Galaxies and 50–50 models during the later stages of reionization at scales of $k < 0.46\,\mathrm{Mpc}^{-1}$ (>14 Mpc) and $k < 0.65\,\mathrm{Mpc}^{-1}$

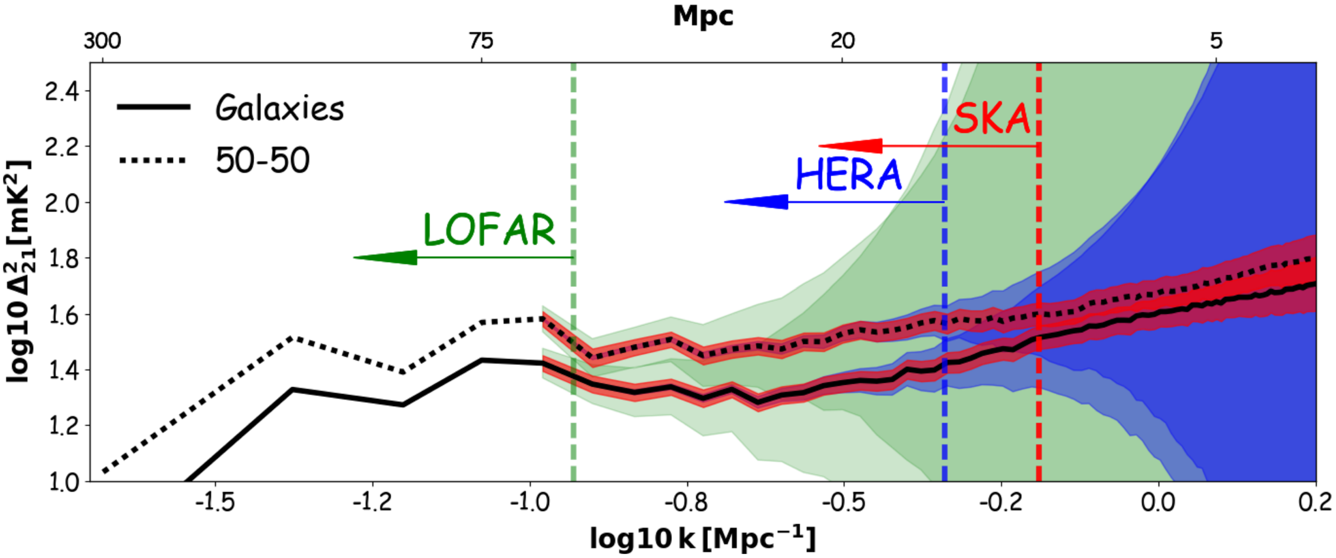

Figure 9. Mock 21 cm EoR power spectrum observations using the same telescope designs and configurations at $z = 8$ and $x_{\rm HI} \sim 30$ per cent from our Galaxies (black solid) and 50–50 (black dotted, tuned to match Galaxies model optical depth τ) models, similar to Fig. 8. Only future 21 cm observations by HERA and SKA will be able to discriminate between these models at their corresponding sensitivity limits.

(>10 Mpc), respectively, as shown by vertical dashed lines in Fig. 9.

Note that we have shown 1σ uncertainties, which is unlikely to be sufficient to robustly discriminate between Galaxies and AGN models. If one instead requires 3σ to distinguish between the models, then LOFAR fails to distinguish between our models, but HERA and SKA are still successful albeit on scales somewhat larger than those obtained with the 1σ limit.

Figs 8 and 9 both illustrate how future 21cm observations could potentially help constrain the nature of the source population. While current observations cannot rule out the 50–50 model, in principle HERA and SKA should be able to do so straightforwardly, assuming that they can reach their target sensitivities. Until these facilities come online, ancillary observations will continue to improve. Hence, comprehensive models that are able to make predictions for, and constrain to, a wide variety of EoR data are vital for optimizing the scientific information extracted from future observations including 21cm data.

4 CONCLUSION

We have presented predictions for the 21cm power spectrum arising from AGN-driven reionization models, and contrasted them with predictions from galaxy-driven models and models with a mixture of sources. The AGN source population is placed into galaxy haloes using a physically motivated prescription based on the G15 AGN observations, deriving a QHOD of AGN at $z = 5.75$ from this and using it to evolve the number of AGN to higher redshifts. This framework is implemented into our time-integrated version of SIMFAST21, which self-consistently accounts for recombinations and the evolution of structure. We have calibrated these AGN models to reproduce ionizing emissivity constraints, and compared them with models in which ionizing radiation is dominated by star-forming galaxies. Our key findings are as follows.

(i) When tuned to match the G15 ionizing emissivity constraints, AGN-only models produce very late reionization at $z \ll 6$ (Fig. 4). If we assume a constant halo occupancy for AGN as is consistent with other observational constraints and models, then the predicted Thomson optical depth is only 0.036, well below *Planck* constraints (see Fig. 5). This strongly disfavours AGN as providing the dominant source for reionizing photons.

(ii) We determine a QHOD that is near unity for very massive haloes, but drops to sub-per cent level for more typical haloes. This is directly interpretable as a duty cycle for AGN. This also explains why reionization is so late in this AGN-only model, because AGN populate massive haloes more frequently and hence their emissivity contribution grows strongly only at late epochs (Fig. 3), thereby not ionizing enough volume to match the optical depth measurements.

(iii) Our results are consistent with those from the AGN-only models by Qin et al. (2017) using the DRAGONS semi-analytic models, who also found that AGN could not dominate reionization. Our Galaxies model is also in broad agreement with their full model, supporting their result that star-forming galaxies can provide sufficient photons as a function of redshift to reionize.

(iv) A model where we assume a constant AGN LF at $z \geq 5.75$ can barely match the *Planck* τ_e, but still reionizes very late, and moreover it is not physically well motivated and disagrees with the measured evolution of the AGN LF at $z \sim 4$–6 (G15). It does, however, result in a global emissivity evolution similar to that assumed in Madau & Haardt (2015), but even in this case we do not confirm their result that such a model is viable, likely because we include the effects of recombinations along with a more sophisticated accounting of the clustering of sources and sinks.

(v) Our AGN-only model produces larger H II bubbles as compared with our Galaxies-only model (see Fig. 6), consistent with results from another semi-numerical model by Kulkarni et al. (2017, Fig. 6). This results in a larger 21 cm power spectrum amplitude by $\sim \times 1.5$–2 as compared with that from the Galaxies-only model (see Fig. 7).

(vi) We examine a model that includes a 50 per cent contribution from galaxies and AGN (assuming a constant QHOD). We find that this model can barely satisfy current τ_e and $x_{\rm HI}$ constraints. At early epochs, the Galaxies contribution dominates the power spectrum, but during the later stages of reionization the quasar contribution is more significant, and the power spectrum deviates more substantially from the Galaxies-only case.

(vii) Future 21 cm observations by LOFAR, HERA and SKA can discriminate between the constant QHOD AGN and Galaxies models during late reionization at scales of $k < 0.21\,\mathrm{Mpc}^{-1}$ ($>$30 Mpc), $k < 0.53\,\mathrm{Mpc}^{-1}$ ($>$12 Mpc) and $k < 1.66\,\mathrm{Mpc}^{-1}$ ($>$4 Mpc), respectively (see Fig. 8). HERA and SKA will also be able to distinguish between our 50–50 and Galaxies-only models, and thus potentially constrain the fractional contribution of AGN to reionization.

(viii) We have assumed an optimistic model for the AGN photon output rate by extrapolating to very low luminosities ($M_{1450} > -18$). There are also suggestions that G15 overestimate the number of high-z AGN and thus their total emissivity (e.g. Parsa et al. 2017). In either scenario, our claim that AGN cannot dominate reionization is further strengthened.

It might still be possible that our AGN-only models could match all EoR observations simultaneously, if we relax some of these models' assumptions. For instance, our AGN-only models depend on two parameters, namely the photon escape fraction $f_{\mathrm{esc,\,AGN}}$ and the black hole formation efficiency A (see equation 4). These results are already obtained using 100 per cent $f_{\mathrm{esc,\,AGN}}$, and it is clear that those models would reionize much earlier if we adopt $f_{\mathrm{esc,AGN}} \gg 100$ per cent, which is not physical. The A parameter has been tuned to allow these models to reproduce the G15 data at $z = 5.75$. If we choose not to calibrate these models to match the G15 data, we then can adopt larger A that results in a smaller QHOD and earlier reionization. For example, the QHOD in the most faint magnitude bin at $z = 5.75$ decreases from $\sim$2.7 per cent to 1.7 per cent as the A increases from 5×10^5 to 10^6. This shows that allowing the AGN-only models to form more efficient black holes (large A) results in a fewer number (less QHOD) of them since the QHOD quantifies the fraction of active haloes with AGN. From Fig. 4, we see that the reionization in the constant LF AGN model (with $A = 10^6$) starts earlier than in the constant QHOD AGN model (with $A = 5 \times 10^5$), but because there is no evolution in the source population (fixed LF), the model reionizes much later than the constant QHOD. It is then clear that if we adopt larger A to form more efficient black holes, our AGN-only models will yield an early reionization. In this case, these models might produce consistent reionization histories and optical depths as compared with the observations. Given the large uncertainties in the ionizing emissivity measurements by G15 and Becker & Bolton (2013), these models might still be consistent with these measurements' 2σ level at $A > 10^6$. We expect that the AGN clustering remains unaffected at a specific neutral fraction for larger A values and hence the future 21 cm observations can still discriminate between our AGN-only versus Galaxy-only models. The AGN-only models also assume that M_{bh}–v_{cir} correlation (equation 4) is valid even at high redshifts. This adds more uncertainties since such a correlation has only been measured in the local Universe. More physically motivated and self-consistent AGN modelling at high redshift is clearly required to understand their formation and evolution as a function of redshift. Analogously to our stellar source model, one may allow the black hole emissivity to scale super-linearly with black hole mass ($R_{\mathrm{ion,AGN}} \propto M_{\mathrm{bh}}^{C}$). This new parameter C would indeed affect the AGN clustering and the corresponding ionized bubble sizes, as previously seen in our star-forming galaxies models ($R_{\mathrm{ion},\star} \propto M_{\mathrm{h}}^{C}$). We leave investigating this dependence for future works.

Improved high-redshift AGN observations are clearly desirable in order to more robustly determine the AGN LF, particularly at the low-luminosity end. The results of such observations can be incorporated straightforwardly into the framework we have presented here, and will provide better constraints on the contribution of AGN to reionization. Our framework illustrates that the QHOD is an effective approach to evolve the number of AGN during the EoR. Our analysis indicates that despite there being potentially more faint AGN than previously believed, star-forming galaxies still dominate the neutral gas topology and ionizing photon budget.

D'Aloisio et al. (2016), Mitra et al. (2016) and Oñorbe et al. (2017) have all independently demonstrated that AGN-only models overheat the IGM, inconsistent with Lyα temperature measurements (Becker et al. 2011), due to the early onset of He II reionization. Finlator et al. (2016) further have shown that these models also overionize the metals when compared with observed metal absorption line measurements (D'Odorico et al. 2013). Our findings corroborate these results via a different approach.

AGN could still be important for reionization because of their long-range heating effects owing to their harder emission spectrum, as well as for setting the shape of the metagalactic ionizing flux that is important for interpreting metal-line absorption data (e.g. Finlator et al. 2016). Early AGN are in and of themselves interesting in order to understand the emergence of supermassive black holes particularly at early epochs. Our results here suggest that future 21 cm experiments will have a key role to play in constraining the amount of AGN activity and its contribution to the metagalactic flux during the EoR.

ACKNOWLEDGEMENTS

We acknowledge helpful discussions with Jonathan Pober and Jonathan Chardin. We thank Girish Kulkarni and Yuxiang Qin for making their models' data available to us. SH is supported by the Deutscher Akademischer Austauschdienst (DAAD) Foundation. RD and SH are supported by the South African Research Chairs Initiative and the South African National Research Foundation. MGS is supported by the South African Square Kilometre Array Project and National Research Foundation. Part of this work was conducted at the Aspen Center for Physics, which is supported by National Science Foundation grant PHY-1066293. RD acknowledges long-term visitor support provided by the Simons Foundation's Center for Computational Astrophysics, as well as the Distinguished Visitor Program at Space Telescope Science Institute, where some of this work was conducted. Computations were performed at the cluster 'Baltasar-Sete-Sois', supported by the DyBHo-256667 ERC Starting Grant, and the University of the Western Cape's 'Pumbaa' cluster.

REFERENCES

Anderson L., Governato F., Karcher M., Quinn T., Wadsley J., 2017, MNRAS, 468, 4077
Barkana R., Loeb A., 2001, Phys. Rep., 349, 125
Barkana R., Loeb A., 2004, ApJ, 609, 2, 474
Becker G. D., Bolton J. S., 2013, MNRAS, 436, 1023
Becker G. D., Bolton J. S., Haehnelt M. G., Sargent W. L. W., 2011, MNRAS, 410, 1096
Becker G. D., Bolton J. S., Madau P., Pettini M., Ryan-Weber E. V., Venemans B. P., 2015, MNRAS, 447, 3402
Berlind A. A. et al., 2003, ApJ, 593, 1
Bian F., Fan X., McGreer I., Cai Z., Jiang L., 2017, ApJ, 837, L12
Bouwens R. J. et al., 2015a, ApJ, 803, 34
Bouwens R. J., Illingworth G. D., Oesch P. A., Caruana J., Holwerda B., Smit R., Wilkins S., 2015b, ApJ, 811, 140

Chardin J., Haehnelt G. M., Aubert D., Puchwein E., 2015, MNRAS, 453, 2943

Chardin J., Puchwein E., Haehnelt G. M., 2017, MNRAS, 465, 3429

Choudhury T. R., Ferrara A., 2005, MNRAS, 361, 577

D'Aloisio A., Upton Sanderbeck P. R., McQuinn M., Trac H., Shapiro P. R., 2017, MNRAS, 468, 4691

D'Odorico V. et al., 2013, MNRAS, 435, 1198

Davé R., Katz N., Oppenheimer B. D., Kollmeier J. A., Weinberg D. H., 2013, MNRAS, 434, 2645

Fan X., Carilli C. L., Keating B., 2006, ARA&A, 44, 415

Ferrarese L., 2002, ApJ, 578, 90

Finkelstein S. L. et al., 2015, ApJ, 810, 71

Finlator K., Thompson R., Huang S., Davé R., Zackrisson E., Oppenheimer B. D., 2015, MNRAS, 447, 2526

Finlator K., Oppenheimer B. D., Davé R., Zackrisson E., Thompson R., Huang S., 2016, MNRAS, 459, 2299

Furlanetto S. R., Zaldarriaga M., Hernquist L., 2004, ApJ, 613, 1

Geil P. M., Wyithe J. S. B., 2009, MNRAS, 399, 1877

Giallongo E. et al., 2015, A&A, 578, A83 (G15)

Glikman E., Djorgovski S. G., Stern D., Dey A., Jannuzi B. T., Lee K.-S., 2011, ApJ, 728, L26

Gnedin N. Y., 2008, ApJ, 673, L1

Grazian A. et al., 2016, A&A, 585, A48

Grazian A. et al., 2017, A&A, 602, A18

Haardt F., Madau P., 2012, ApJ, 746, 125

Hassan S., Davé R., Finlator K., Santos M. G., 2016, MNRAS, 457, 1550

Hassan S., Davé R., Finlator K., Santos M. G., 2017, MNRAS, 468, 122

He W. et al., 2017, PASJ, preprint (arXiv:1704.08461)

Hopkins P. F., Richards G. T., Hernquist L., 2007, ApJ, 654, 731

Iliev I. T., Mellema G., Ahn K., Shapiro P. R., Mao Y., Pen U.-L., 2014, MNRAS, 439, 725

Japelj J. et al., 2017, MNRAS, 468, 389

Jiang L. et al., 2016, ApJ, 833, 222

Khaire V., Srianand R., Choudhury T. R., Gaikwad P., 2016, MNRAS, 457, 4051

Kim Y. et al., 2015, ApJ, 813, L35

Kuhlen M., Faucher-Giguére C.-A., 2012, MNRAS, 423, 862

Kulkarni G., Choudhury T. R., Puchwein E., Haehnelt M. G., 2017, MNRAS, 469, 4283

Loeb A., Barkana R., 2001, ARA&A, 39, 19

Ma X., Kasen D., Hopkins P. F., Faucher-Giguère C.-A., Quataert E., Kereš D., Murray N., 2015, MNRAS, 453, 960

Mao J., Kim M., 2016, ApJ, 828, 96

McGreer I. D., Mesinger A., DOdorico V., 2015, MNRAS, 447, 499

McQuinn M., Lidz A., Zaldarriaga M., Hernquist L., Hopkins P. F., Dutta S., Faucher-Giguère C.-A., 2009, ApJ, 694, 842

Madau P., Haardt F., 2015, ApJ, 813, L8

Majumdar S., Mellema G., Datta K. K., Jensen H., Choudhury T. R., Bharadwaj S., Friedrich M. M., 2014, MNRAS, 443, 2843

Masters D. et al., 2012, ApJ, 755, 169

Mesinger A., Furlanetto S., Cen R., 2011, MNRAS, 411, 955

Micheva G., Iwata I., Inoue A. K., 2017, MNRAS, 465, 302

Mitra S., Ferrara A., Choudhury T. R., 2013, MNRAS, 428, L1

Mitra S., Choudhury T. R., Ferrara A., 2016, MNRAS, preprint (arXiv:1606.02719)

Mutch S. J., Geil P. M., Poole G. B., Angel P. W., Duffy A. R., Mesinger A., Wyithe J. S. B., 2016, MNRAS, 462, 250

Oñorbe J., Hennawi J. F., Lukić Z., Walther M., 2017, ApJ, preprint (arXiv:1703.08633)

Oppenheimer B. D., Davé R., Finlator K., 2009, MNRAS, 396, 729

Paardekooper J., Khochfar S., Vecchia D. C., 2015, MNRAS, 451, 2563

Parsa S., Dunlop J. S., McLure R. J., 2017, MNRAS, preprint (arXiv:1704.07750)

Parsons A., Pober J., McQuinn M., Jacobs D., Aguirre J., 2012, ApJ, 753, 81

Pober J. C. et al., 2013, AJ, 145, 65

Pober J. C. et al., 2014, ApJ, 782, 66

Qin Y. et al., 2017, MNRAS, 472, 2009

Ricci F., Marchesi S., Shankar F., La Franca F., Civano F., 2017, MNRAS, 465, 1915

Robertson B. E. et al., 2013, ApJ, 768, 71

Robertson B. E., Ellis R. S., Furlanetto S. R., Dunlop J. S., 2015, ApJ, 802, L19

Santos M. G., Ferramacho L., Silva M. B., Amblard A., Cooray A., 2010, MNRAS, 406, 2421

Schaye J., Carswell R. F., Kim T.-S., 2007, MNRAS, 379, 1169

Schirber M. Bullock J. S., 2003, ApJ, 584, 110

Shankar F., Weinberg D. H., Miralda-Escudé J., 2009, ApJ, 690, 1

Shankar F., Mathur S., 2007, ApJ, 660, 1051

Shapiro P. R., Giroux M. L., 1987, ApJ, 321, L107

Sobacchi E., Mesinger A., 2014, MNRAS, 440, 1662

Telfer R. C., Zheng W., Kriss G. A., Davidsen A. F., 2002, ApJ, 565, 773

Tremaine S. et al., 2002, ApJ, 574, 740

Vanzella E. et al., 2016, ApJ, 825, 41

Vasei K. et al., 2016, ApJ, 831, 38

Wise J. H., Demchenko V. G., Halicek M. T., Norman M. L., Turk M. J., Abel T., Smith B. D., 2014, MNRAS, 442, 2560

Worseck G., Prochaska J. X., Hennawi J. F., McQuinn M., 2016, ApJ, 825, 144

Wyithe J. S. B., Loeb A., 2003, ApJ, 595, 614

Yajima H., Choi J.-H., Nagamine K., 2011, MNRAS, 412, 411

Yoshikawa K., Taruya A., Jing Y. P., Suto Y., 2001, ApJ, 558, 520

Zahn O., Mesinger A., McQuinn M., Trac H., Cen R., Hernquist L. E., 2011, MNRAS, 414, 727

Zel'Dovich Y. B., 1970, A&A, 5, 84

Planck Collaboration XLVII, 2016, A&A, 596, A108

This paper has been typeset from a TEX/LATEX file prepared by the author.